

# Photophysical Changes of Pyranine Induced by Surfactants: Evidence of Premicellar Aggregates

Ramon Barnadas-Rodríguez and Joan Estelrich\*

Departament de Físicoquímica, Facultat de Farmàcia, Universitat de Barcelona, Avda. Joan XXIII s/n, 08028-Barcelona, Catalonia, Spain

Received: July 31, 2008; Revised Manuscript Received: December 11, 2008

We studied photophysical changes of pyranine in different surfactant environments using spectrophotometry, steady-state fluorescence, and time-resolved fluorescence lifetime. The effect of surfactants on such properties varied as a function of the surfactant charge. Whereas anionic surfactants did not show any kind of interaction, the nonionic surfactant Triton X-100 produced spectral changes in the dye, as a consequence of the shift of equilibrium between its excited species. In the case of fluorescence, these changes allowed the critical micellar concentration of the surfactant to be determined. However, the most important features were obtained from the interaction with cationic surfactants of the *n*-alkyl trimethylammonium bromides. Such interactions enabled the formation of premicellar aggregates to be determined. In addition, three or four critical concentrations could be defined, which were dependent on the length of the hydrocarbon chain. One of these was the critical micellar concentration of the surfactant. The remaining two or three were in the very dilute concentration domain from which several types of premicellar aggregates are formed. However, the interaction with dodecyltrimethylammonium bromide at submicellar concentrations evidenced a quenching effect of a different nature (either static or combined), depending on the surfactant concentration. By deconvoluting the overall pyranine fluorescence emission spectrum into a sum of overlapping Lorentzian–Gaussian functions, the principal microenvironments of the pyranine molecules can be ascertained. Fluorescence data are consistent with the location of pyranine in a variety of sites, including partitioning that may be influenced by electrostatic and  $\pi$ -cation interactions in aqueous micelles.

## 1. Introduction

Pyranine (8-hydroxypyrene-1,3,6-trisulfonate, trisodium salt) (HPTS) is a water-soluble fluorescent molecule that belongs to the photoacids. Like all photoacids, HPTS discharges a proton when excited to its first electronic singlet state. Consequently, its acidity can be enhanced through excitation. In this way, the  $pK_a$  of HPTS decreases from 7.4 in the ground-state to 1.4 in the first excited state. Thus, HPTS is a weak acid in the ground-state but a very strong acid in the excited state. In addition, an excited HPTS rapidly transfers a proton to a water molecule, even in highly acidic media (e.g., pH 2).<sup>1,2</sup>

The absorption spectrum of HPTS is due to its protonated (ROH) and deprotonated (RO<sup>−</sup>) forms, whereas the fluorescent properties emanate from the corresponding excited states, ROH\* and RO<sup>−</sup>\*. The absorption maximum of ROH is 403 nm, and that of RO<sup>−</sup> is 454 nm. The maximum fluorescence of the RO<sup>−</sup>\* form, corresponding to the lowest excited-state of the conjugated base, is 510–515 nm. The emission maximum of the lowest excited-state of ROH\* is 440–445 nm. As stated above, the prototropic equilibrium of the electronically excited states has a  $pK_a^*$  that is much lower than that of the ground state. This means that the OH group of the excited HPTS is much more acidic than that of the ground state.

Photophysical properties of HPTS change with changes in the environment. Consequently, when HPTS interacts with other species, its spectroscopic properties change. For example, it is known that the interaction of the dye with positive molecules, as shown by Ray and Nakahara using octadecylamine,<sup>3</sup> leads

to an important change in the emission spectrum of HPTS. Barrash-Shifftan et al. have shown that not only the maximum ROH\* fluorescence but also the UV–visible absorption spectra are solvent-dependent.<sup>4</sup>

The ground- and excited-state proton transfer of HPTS has been studied, among other species, in the presence of surfactants.<sup>5–10</sup> Surfactant monomers in solution self-assemble into aggregates of various structures (micelles), which are widely used as reaction media, model colloids, rudimentary models of biological lipid membranes, and, in particular, solubilizers for sparingly soluble compounds. The use of micelles as drug delivery vehicles also helps to minimize drug degradation and adverse drug responses.<sup>11</sup> In this context, precise knowledge about the size of the aggregates and a quantitative determination of the critical micellar concentration (CMC) is indispensable. Many methods have been developed to determine CMCs. The most common are based on measurements of surface tension, conductivity, and dynamic light scattering.<sup>12</sup> More recently, fluorescence correlation spectroscopy has been used as an alternative method for characterizing the self-aggregation behavior of surfactants.<sup>13</sup> The formation of micelles is preceded by the creation of smaller assemblies in different phases of aggregation. These are known as premicellar aggregates. Although the study of premicellar aggregation entails meeting the high requirements of working with precision at such extremely low concentrations and, consequently, with such low values of the experimental physicochemical property, the existence of self-aggregation prior to micelle formation has been experimentally observed.<sup>13–21</sup> Recently, a theoretical two-state model was developed to study the aggregation mechanism.<sup>22</sup>

\* To whom correspondence should be addressed. Phone: (+ 34) 934024559; fax: (+ 34) 934035987; e-mail: joanestelrich@ub.edu.

Surfactants, especially in micellar form, affect the spectral characteristics of dyes (leading to a shift in the wavelength of maximum absorption or emission, to changes in the fluorescence quantum yield, or all of these).<sup>15,23–27</sup> In some cases, this property has been used to determine the CMC by spectrophotometry. Spectroscopic CMC determination relies on the use of a probe molecule that readily partitions into micelles and whose spectral characteristics change in some way within the micelle. Furthermore, it is possible to locate the region of solubilization of the dye in the micelle by observing differences in the positions and shapes of the absorption and fluorescence bands, as well as variations in fluorescence lifetime decays.<sup>28–30</sup>

In this paper, we studied the interaction of HPTS with cationic, anionic, and nonionic surfactants, at sub- and supramicellar concentrations, in aqueous medium at different NaCl concentrations. Fluorescence studies rely on characterizing the emission spectrum after excitation at 350 nm, by means of its component bands. We also analyzed the evolution of the maxima corresponding to the ROH\* and RO<sup>−</sup>\* forms of HPTS.

## 2. Experimental Section

**Materials.** Pyranine, or 8-hydroxy-1,3,6-pyrenetrisulfonic acid trisodium salt (HPTS), and Triton X-100 (TX100) were purchased from Sigma (St. Louis, MO). Sodium dodecyl sulfate (SDS) and dodecyltrimethylammonium bromide (DTAB) were from Fluka (Buchs, Switzerland). Sodium 1-dodecanesulphonate (SDoS) was from Lancaster (Morecambe, UK). Tetradecyltrimethylammonium bromide (TTAB) and hexadecyltrimethylammonium bromide (HTAB) were purchased from ICN Biomedicals Inc. (Aurora, OH). All other reagents were of analytical grade. Solutions were made in ultrapure water (Milli Q reverse osmosis system, 18.3 MΩ·cm resistivity).

**Methods. Sample Preparation.** Solutions of HPTS containing different concentration of surfactants were obtained by adding the required amount of concentrated stock solutions of surfactants, containing HPTS at the same concentration and pH as the sample.

**Fluorescence Measurements and Analyses of Steady-state Fluorescent Spectra.** Fluorescence measurements were performed in a SLM Aminco Series 2 spectrofluorimeter. After excitation at 350 nm, fluorescence emission spectra were recorded from 360 to 650 nm using a resolution of 1 nm and a bandpass of 2 nm for excitation and emission. When not specified, the concentration of HPTS solutions was 6 μM at pH 3.5 or 9.4. Acidic solutions showed no variation of their pH during acquisitions. When they were performed at pH 9.4, the pH of the stock solutions were adjusted before the acquisition, continuously measured, and, if necessary, readjusted in order to ensure that no significant change of the pH took place.

Emission spectra were analyzed by deconvolution into overlapping mixed Gaussian–Lorentzian curves with a nonlinear least-squares multi peaks fitting procedure that uses an iterative Marquard–Levenberg fitting algorithm (Grams 3.2, Galactic, Salem, NH). The component curves were characterized by their center, area, and percent area. In many cases a unique solution is not possible, due to fits involving multiple adjustable parameters. In the case of HPTS, this does not represent a problem when spectra changes do not imply any shift in the main bands. In this case, changes are caused only by modifications of the equilibrium between ROH\* (2 component bands) and RO<sup>−</sup>\* (2 component bands) species. The intensity changes of the original spectra are well described by the overall variation in the area of the ROH\* and RO<sup>−</sup>\* bands. In contrast, when the experimental spectra of HPTS undergo modifications in the

emission maxima, multiple, statistically equivalent minima of the fitting exist. As described in the literature,<sup>31</sup> and to circumvent this uncertainty as far as possible, several features were chosen as the control test to ensure the goodness of the deconvolution: (i) the use of a minimum number of component bands; (ii) the reproducibility of the final results for the center and the area of the peaks; (iii) a minimum value in the  $\chi^2$  parameter; (iv) a random residual plot, equal to the instrumental noise and with no systematic features; and (v) a maximum value for the square of the multiple correlation coefficient,  $r^2$ .

**Time-resolved Fluorescence Measurements.** The lifetime determination of the RO<sup>−</sup>\* form was performed using an EasyLife LS instrument (PTI Technologies, Birmingham, NJ). Samples at pH 3.5 or pH 9.4 were excited at 340 and 280 nm, respectively, with a picosecond diode laser in order to achieve a high signal-to-noise ratio, since HPTS fluorescence is pH-dependent. The pH of stock solutions was monitored and, if necessary, readjusted. Emission at wavelengths higher than 530 nm was observed through a cutoff filter (Edmund Optics Inc. Barrington, NJ). Colloidal silica (Ludox) was employed to obtain the instrument response function, and lifetimes were obtained by deconvolution routines using PTI software (FeliX32).

**Absorbance Measurements and Analyses.** Absorption spectra of 12 μM HPTS solutions in the presence or absence of surfactants were acquired with a Shimadzu UV-2401 PC spectrophotometer at a resolution of 0.2 nm. The HPTS concentration was double that used in fluorescence experiments, in order to minimize experimental error. The spectra maxima were obtained after smoothing to eliminate the effect of instrumental noise. The same pH control described for fluorescence measurements was performed in these samples.

**Light Scattering Analysis.** Vesicle size determination was performed using a Zetasizer NanoZS90 (Malvern, UK) at 25 °C using nondiluted samples. This device automatically regulates the intensity of the incident light on the detector, allowing the analysis of concentrated samples. Therefore, several orders of sample concentration can be used, this fact avoiding changes in the absolute concentration of the components, which should alter the equilibrium between the phases.

**pH Determination.** pH was measured at room temperature using a GLP22 pH-meter (Crison, Barcelona) and adjusted by adding the appropriate volumes of HCl or NaOH solutions to the samples.

## 3. Results

**Effect of Triton X-100 on the Spectral Properties of HPTS.** The absorption spectra of HPTS in TX100 solutions of various concentrations at different concentrations of NaCl did not show much variation. This indicates the low absorbance sensitivity to changes in surfactant concentration.

The inset of Figure 1 shows fluorescence emission spectra of 6 μM HPTS in water at pH 3.5 in the absence and presence of nonionic surfactant TX100 at concentrations ranging from 0 to 50 mM. There was no shift in the position of the maxima corresponding to ROH\* (441 ± 1 nm) and RO<sup>−</sup>\* (511 ± 1 nm) forms of the dye. However, an increment in the 441 band and a 511 band decrease were concomitant to a rise in surfactant concentration. The same effect occurred at NaCl concentrations of 50, 155, and 300 mM. In these cases, due to the effect of the Na<sup>+</sup> cation on the equilibrium of the excited species of HPTS,<sup>32</sup> the relative intensities of the ROH\* and RO<sup>−</sup>\* bands were different. These changes in the spectra can be represented by means of the ratio between the fluorescence intensity at 511 and 441 nm. Figure 1 shows this ratio compared to that obtained

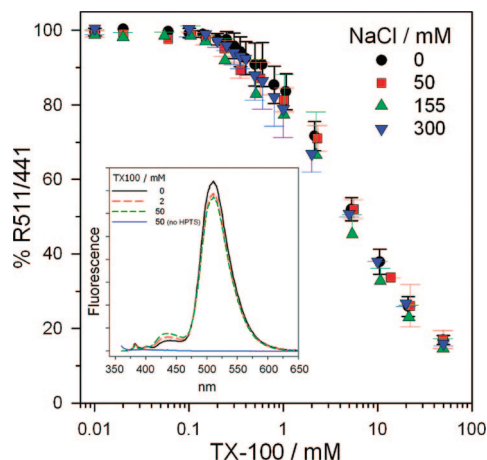


**Figure 1.** Ratio of the fluorescence emission of HPTS at 511 and 441 nm as a function of TX100 concentration at different NaCl concentrations. The ratio is expressed as percentage of the ratio obtained in absence of the surfactant. (Results: mean  $\pm$  std;  $n \geq 3$ ). Inset: fluorescence spectra of 6  $\mu$ M HPTS in water at several TX100 concentrations and of a blank performed with TX100 at 50 mM (with no HPTS). Samples were excited at 350 nm.

in the absence of surfactant, that is, the percentage of the initial ratio (% R511/441), as a function of TX100 concentration for different NaCl concentrations. All solutions behaved similarly: at low TX100 concentrations there was no change in the % ratio, whereas the ratio decreased at high surfactant concentrations. The interception of the slope of the different curves with the initial value of the ratio (100%) took place at the same TX100 concentration for all the NaCl curves:  $0.227 \pm 0.040$  mM. In the 0–50 mM TX100 concentration range, the total area of fluorescent spectra did not vary more than 4% from the area in the absence of the surfactant.

**Effect of Dodecyltrimethylammonium Bromide on Spectral Properties of HPTS.** The absorption spectrum of HPTS in the presence of DTAB at pH 3.5 exhibited modifications indicating that the ground-state forms had experienced a change of environment (Figure 2a inset). Because of the fact that the  $pK_a$  of the dye is 7.4, at pH 3.5<sup>33</sup> the major species in the ground-state was the ROH form. In these conditions, the position of the maxima and their absorbance values changed with DTAB concentration. However, there was no increment of the band corresponding to the RO<sup>−</sup> form. When the surfactant concentration was increased to 7 mM approximately, the maximum located at 403 nm shifted 2 nm to longer wavelengths (Figure 2a). At the same time, the intensity of this peak diminished by about 15% of its initial value in pure water (see Figure SI.1a in the Supporting Information). At higher DTAB concentrations, absorbance rose gradually and became 110% of the initial value when DTAB was 14 mM.

Figure 2b inset shows the changes of the absorption spectrum of HPTS in the presence of DTAB at pH 9.4. At this pH, the major species in the ground-state was RO<sup>−</sup>. As is the case for the ROH, any increment in DTAB concentration did not enhance the conjugate species band. In a first step, the maximum RO<sup>−</sup> form located in pure water at 454 nm shifted to 460 nm when the DTAB concentration was increased to 7 mM. After that, the behavior was different from that of the ROH form (Figure 2b). From this concentration to 14 mM, the absorbance maximum returned to the initial position. Another difference from the ROH species was the appearance of turbidity when the DTAB concentration ranged from approximately 5 to 10 mM. The turbidity was due to the large-scale scattering produced

by the colloidal particles formed by the association of the dye with the surfactant. The determination of such particles by dynamic light scattering afforded radii centered at 250 nm at the 2.5–7.5 mM DTAB range. Below 2.5 mM, no measurable signal was detected by the instrument. Between 7.5 and 14 mM, the peak at  $\sim 250$  nm disappeared, and above 14 mM a new peak was visualized at  $\sim 5$  nm, indicating the formation of micelles. To avoid the effect of scattering on absorbance values, the spectral baseline was subtracted from the experimental values. The absorbance value of the 454 nm peak progressively decreased to 93% of the initial value when the DTAB concentration was changed from 1 to 14 mM. This trend was broken in the 5–10 mM range, due to the aforementioned turbidity of the samples. Consequently, a local absorption maximum was observed (see Figure SI.1b in the Supporting Information).

The fluorescent spectrum of HPTS at pH 3.5 changed significantly with the DTAB concentration (Figure 3, inset). In a first approximation, the most relevant variations were as follows: (a) from 0 to approximately 1 mM of DTAB there was a decrease in the emission intensity of the RO<sup>−</sup>\* and ROH\* species; (b) in the 1–7 mM range, a great diminution of the RO<sup>−</sup>\* fluorescence was observed; (c) from 7 to 14 mM there was an intense shift in the emission maxima of the ROH\* and RO<sup>−</sup>\* forms (from 441 to 427 nm and from 511 to 528 nm, respectively) and a progressive increment in fluorescence; and (d) the position of the emission maxima and the fluorescence intensity became practically constant between approximately 14 and 50 mM DTAB (the maximal concentration assayed).

At pH 9.4, when practically the unique species in the ground and excited states is RO<sup>−</sup>, the fluorescent spectrum of the deprotonated band exhibited a similar behavior than that observed at pH 3.5. The major difference was the emergence of the ROH\* band (with its maximum located at 424 nm) at a DTAB concentration equal or higher than 14 mM, a band that was not present at any lower tensioactive concentration.

Changes in ROH\* and RO<sup>−</sup>\* emissions were due to the quenching effect induced by the surfactant. Fluorophore quenching is frequently calculated by a Stern–Volmer plot. The ratio between the fluorescent intensities of a species in the absence ( $F_0$ ) and presence ( $F$ ) of the quencher is displayed as a function of quencher concentrations. In the simplest form of quenching, the following equation is used:

$$\frac{F_0}{F} = 1 + K_{SV}Q \quad (1)$$

where  $K_{SV}$  is the Stern–Volmer quenching constant of the fluorophore, and  $Q$  is the concentration of the quencher. This constant does not presuppose any specific mechanism of quenching (neither static nor dynamic).

Figure 3 shows the quenching produced by DTAB on RO<sup>−</sup>\* and ROH\* at pH 3.5 and 9.4. It is evident that, at pH 3.5 from 0 to approximately 1 mM of surfactant, the same quenching effect was produced in both species. This visual evidence was confirmed by the fact that the quenching constants of both species, obtained by linear regression, were equivalent:

$$K_{RO^-*} = 0.271 \pm 0.053 \text{ mM}^{-1}; r^2 = 0.9434 \quad (10)$$



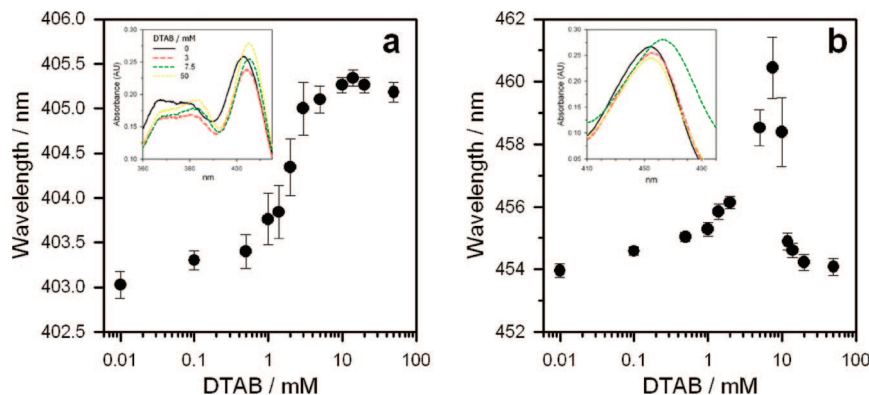


**Figure 2.** Position of the maxima of absorption of HPTS 12  $\mu$ M at pH 3.5 (a) and pH 9.4 (b) as a function of the DTAB concentration (results: mean  $\pm$  sem;  $n \geq 5$ ). Inset: corresponding absorption spectra.

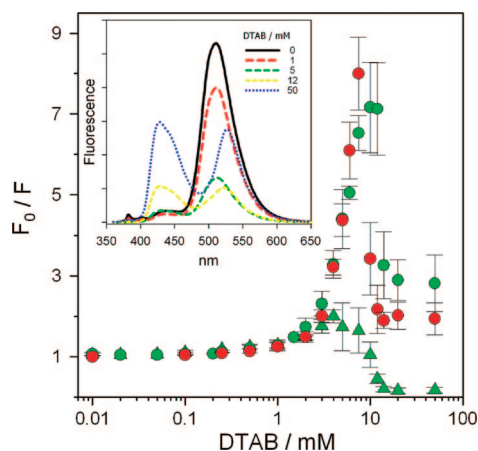


**Figure 3.** Ratio of initial fluorescence ( $F_0$ ) at 511 nm (circles) and 441 nm (triangles) to that obtained in presence of DTAB ( $F$ ) at pH 3.5 (green) or 9.4 (red) (Results: mean  $\pm$  std;  $n \geq 3$ ). Inset: fluorescence emission spectra of HPTS at pH 3.5 as a function of DTAB concentration.

$$K_{\text{ROH}^*} = 0.228 \pm 0.014 \text{ mM}^{-1}; r^2 = 0.9847 \quad (11)$$

The linear dependence of the fluorescent ratio of  $\text{ROH}^*$  at pH 3.5 was maintained until a surfactant concentration of 4 mM was reached. Between 4 and approximately 10 mM of surfactant, the  $\text{ROH}^*$  intensity ratio showed a high uncertainty and a tendency to decrease. In contrast, at the previous pH and between 1 and 7.5 mM of DTAB,  $\text{RO}^{*-}$  deviated positively from the linear dependence found between 0 and 1 mM of DTAB. For any concentration higher than 7.5 mM of DTAB, the Stern–Volmer plot was affected by the important shift in the emission maxima of  $\text{RO}^{*-}$  and  $\text{ROH}$ . Consequently, the ratio did not represent the quenching effect on both species with accuracy.

At pH 9.4, the  $\text{RO}^{*-}$  form showed a similar evolution than that displayed at pH 3.5 (Figure 3), but, at the basic pH, the initial linear quenching range was slightly higher. The quenching constant of  $\text{RO}^{*-}$ , obtained by linear regression between 0 and 2 mM of DTAB was:

$$K_{\text{RO}^{*-}(\text{pH } 9.4)} = 0.261 \pm 0.026 \text{ mM}^{-1}; r^2 = 0.9954 \quad (12)$$

To circumvent the effect of the shift of the maxima of emission of  $\text{RO}^{*-}$  and  $\text{ROH}$  forms, and, moreover, to obtain the relative quantum yield of each one of the excited forms of

HPTS, the emission spectra obtained at different DTAB concentrations at pH 3.5 and 9.4 were fitted to their component bands. Some examples are shown in Table 1 and in Figure 4, panels a and b. At pH 3.5 the  $\text{ROH}^*$  experimental band was described by two component bands up to a DTAB concentration of 6 mM. In the 1.4 to 6 mM range there was a small and progressive blue shift of both bands, and at DTAB concentrations above 6 mM the experimental  $\text{ROH}^*$  band was composed of three bands. The position of these three bands, centered at  $422 \pm 1$ ,  $439 \pm 1$ , and  $462 \pm 3$  nm (the results are the mean of different DTAB concentrations) did not significantly change when the DTAB concentration was further increased. Deconvolution of the  $\text{RO}^{*-}$  experimental band at pH 3.5 and 9.4 rendered two component bands, which underwent a progressive red shift as the DTAB concentration increased. This shift was not great at DTAB concentrations equal to or lower than 6 mM but was significant at higher concentrations.

The relative quantum yield of HPTS and their excited species were calculated from the ratio of the area of the corresponding component peaks over the total area obtained in the absence of DTAB. After a small and progressive decrease in fluorescence at low surfactant concentrations (Figure 4, panels c and d), the relative quantum yield of the dye fell between 1 and 7.5 mM of DTAB and recovered its initial fluorescence in the 10–14 mM range. As can be observed, the quenching effect was caused mainly by the decrease in the fluorescence of the  $\text{RO}^{*-}$  species, which was predominant at the two working pHs ( $\text{ROH}^*$  fluorescence at pH 9.4 was, initially, less than 1% and became practically 0 at low DTAB concentrations). The further increase in relative quantum yield was a consequence of the rise in the fluorescence of both  $\text{ROH}^*$  and  $\text{RO}^{*-}$  forms. When the total fluorescence was recovered, there was significant growth in the fluorescence contribution of the protonated form of HPTS. This is also true for pH 9.4, the final relative quantum yield being about 15% of the total fluorescence. The percentage area of the 422 nm component band significantly increased with DTAB concentration between approximately 6 and 14 mM. At higher surfactant concentrations it reached a plateau at a value of around 11%.

In addition to the steady state experiments, fluorescence lifetime decays of the  $\text{RO}^{*-}$  form were acquired at different DTAB concentrations (See Figure SI.2 in the Supporting Information). The lifetime of such species in pure water at pH 3.5 and 9.4 did not vary ( $5.38 \pm 0.18$  and  $5.42 \pm 0.06$  ns, respectively) at any DTAB concentration under 1–2 mM (Figure 5). However, between 1–2 and 7.5 mM of DTAB there was a progressive diminution of the lifetime, and the linear regression of the data of this interval provided a straight line

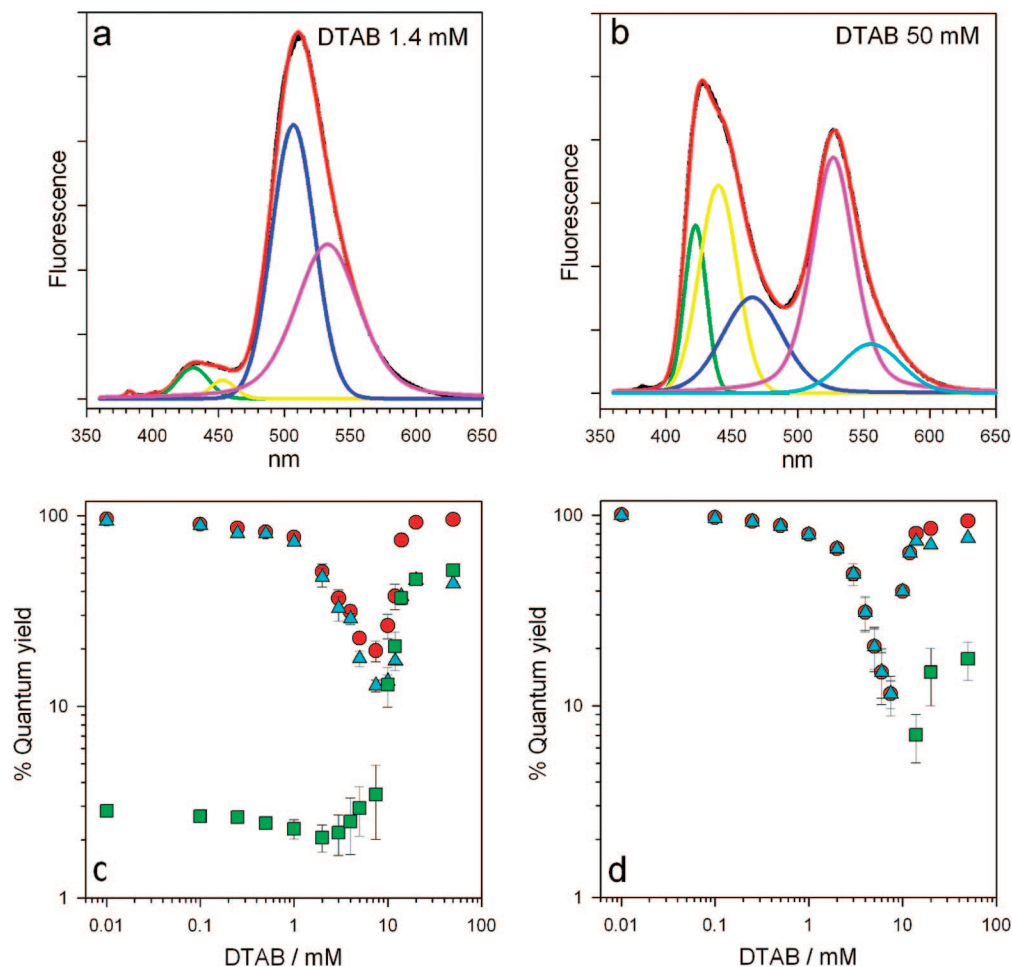


**Figure 4.** Original spectra and component bands of HPTS in water at pH 3.5 at (a) 1.4 and (b) 50 mM of DTAB. Relative quantum yield of HPTS (red circles), ROH\* (green squares) and RO\* (cyan triangles) species in water at (c) pH 3.5 and (d) pH 9.4, as a function of DTAB concentration. The values were obtained from the areas of the corresponding component peaks and referred to the area of the dye in absence of the surfactant. (results: mean  $\pm$  std;  $n \geq 3$ ).

**TABLE 1: Center (nm) and Percentage of Area of Component Bands of the Protonated (ROH\*) and Deprotonated (RO\*) Species of HPTS as a Function of DTAB Concentration**

DTAB/mM	ROH* BAND						RO* BAND			
	Peak 1		Peak 2		Peak 3		Peak 4		Peak 5	
	center	% area	center	% area	center	% area	center	% area	center	% area
0			433 $\pm$ 1	2.34 $\pm$ 0.07	453 $\pm$ 1	0.76 $\pm$ 0.09	506 $\pm$ 1	47.1 $\pm$ 0.5	531 $\pm$ 1	49.8 $\pm$ 0.6
2			426 $\pm$ 1	2.29 $\pm$ 0.50	449 $\pm$ 1	3.02 $\pm$ 0.12	507 $\pm$ 1	19.7 $\pm$ 4.5	533 $\pm$ 1	17.8 $\pm$ 3.5
10	423 $\pm$ 1	3.92 $\pm$ 1.05	439 $\pm$ 2	8.00 $\pm$ 2.73	463 $\pm$ 8	6.54 $\pm$ 2.18	521 $\pm$ 3	13.6 $\pm$ 1.2	569 $\pm$ 8	1.60 $\pm$ 1.29
50	422 $\pm$ 1	11.8 $\pm$ 0.6	439 $\pm$ 1	23.5 $\pm$ 2.1	461 $\pm$ 5	20.4 $\pm$ 1.8	527 $\pm$ 1	27.6 $\pm$ 9.5	543 $\pm$ 12	19.3 $\pm$ 10.7

with a slope of  $0.100 \pm 0.012 \text{ mM}^{-1}$  ( $r^2 = 0.9419$ ) when pH was 3.5 and  $0.120 \pm 0.024 \text{ mM}^{-1}$  ( $r^2 = 0.9658$ ) at pH 9.4. An additional increment of DTAB caused a drop in the  $\tau_0/\tau$  value, that is, an increment in the lifetime. At any DTAB concentration higher than 14 mM the lifetime was  $8.79 \pm 0.78 \text{ ns}$  at pH 3.5 and  $6.87 \pm 0.30 \text{ ns}$  at pH 9.4.

Like TX100, spectral changes in the steady state fluorescence spectra of HPTS in the presence of DTAB can be represented as a percentage ratio of the maximal fluorescence (due to the fact that at pH 9.4 not enough ROH\* signal is obtained at DTAB concentrations lower than 14 mM, this ratio could not be calculated). Figure 6 shows the results of the absolute and relative values of the R511/441 ratio at 0, 10, 50, 155, and 300 mM concentrations of NaCl ( $r^2 = 0.9788$ ). No significant differences due to the effects of the salt were observed, and a unique curve fitted the experimental points. The intersection of

the slope of the curve with 100% of the relative ratio took place at a DTAB concentration,  $C_1$ , of  $1.26 \pm 0.17 \text{ mM}$ . As there was a significant fluorescent shift in the intense RO\* band, the ratio between the intensity at 511 and 528 nm was also calculated. At pH 3.5 the corresponding percentage ratio, % R511/528 (referring to that obtained in pure water), showed that the effect of DTAB concentration on RO\* fluorescence in this case was modulated by the presence of NaCl (Figure 7). As can be observed, the sigmoid curve ( $r^2 = 0.9991$ ) obtained with the fluorescence of RO\* species in the absence of salt was modified in a concentration-dependent manner. From the data and for each NaCl concentration assayed, two concentrations can be calculated: (1) the DTAB concentration,  $C_2$ , located at the intersection of the slope of the curve with the initial value of the ratio (100% of R511/528) and (2) the DTAB concentration,  $C_3$ , located at the intersection of the slope of the curve

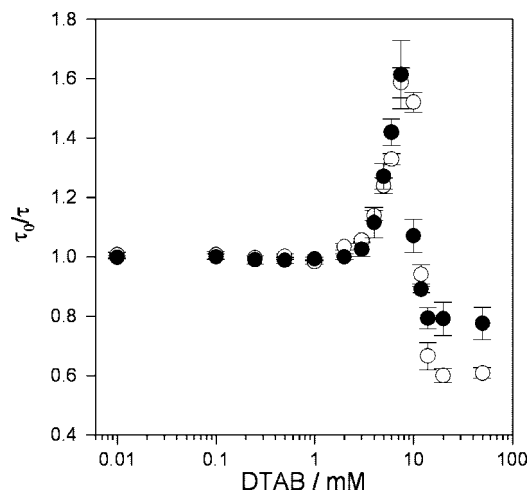


**Figure 5.** Dependence of lifetime of  $\text{RO}^-*$  upon DTAB concentration at pH 3.5 (white circles) and pH 9.4 (black circles). (Results: mean  $\pm$  std;  $n \geq 3$ ).

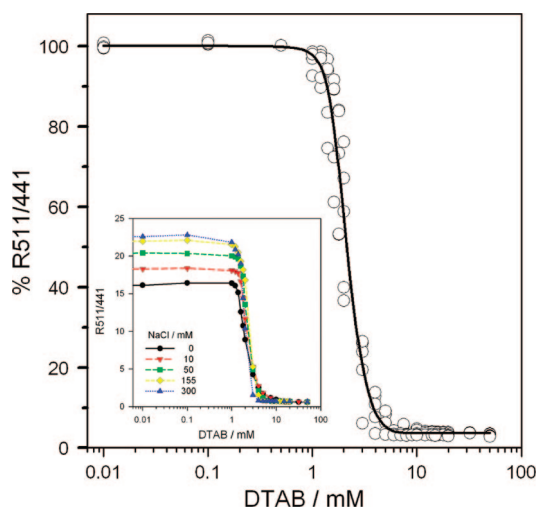


**Figure 6.** Percentage ratio of the fluorescence emission of HPTS at 511 and 441 nm as a function of DTAB concentration at 0, 10, 50, 155, and 300 mM of NaCl at pH 3.5. The curve was obtained from all the experimental points. Inset: the corresponding absolute values.

with the final value of the ratio ( $45 \pm 1\%$  of the initial ratio). In pure water at pH 3.5, the experimental values of  $C_2$  and  $C_3$  were  $5.74 \pm 0.05$  mM and  $14.5 \pm 0.25$  mM, respectively. From the data, the following semilogarithmic equations, which describe the dependence of these points on the NaCl concentration, could be efficiently fitted:

$$C_2/\text{mM} = 8.93 - 1.16 \ln([\text{NaCl}] + 9.54); r^2 = 0.9704 \quad (2)$$

$$C_3/\text{mM} = 21.9 - 3.20 \ln([\text{NaCl}] + 9.54); r^2 = 0.9935 \quad (3)$$

At pH 9.4 the  $\% \text{R511/528}$  obtained in water showed a similar trend as that displayed at pH 3.5 (see Figure SI.3 in the Supporting Information), although the following minor differences could be appreciated: (1) the DTAB concentration  $C_2$  was  $4.86 \pm 0.37$ ; (2) the DTAB concentration  $C_3$ ,  $14.1 \pm 0.12$  mM, was obtained after a local minimum of the fluorescent ratio located at, approximately, 10 mM of DTAB; and (3) the final value of the ratio was higher ( $54.0 \pm 1\%$ ).

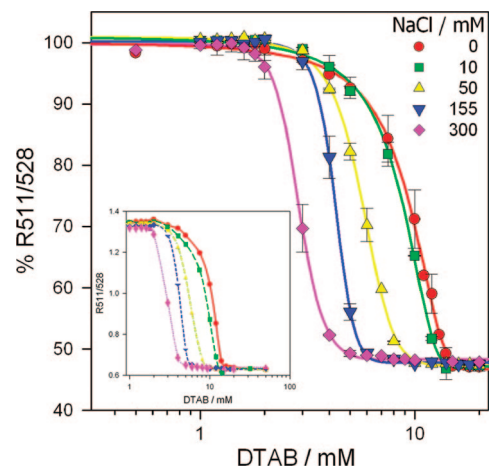


**Figure 7.** Percentage ratio of the fluorescence emission of HPTS at 511 and 528 nm at pH 3.5 as a function of DTAB concentration at 0, 10, 50, 155, and 300 mM of NaCl. (Results: mean  $\pm$  std;  $n \geq 3$ ). Inset: the corresponding absolute values.

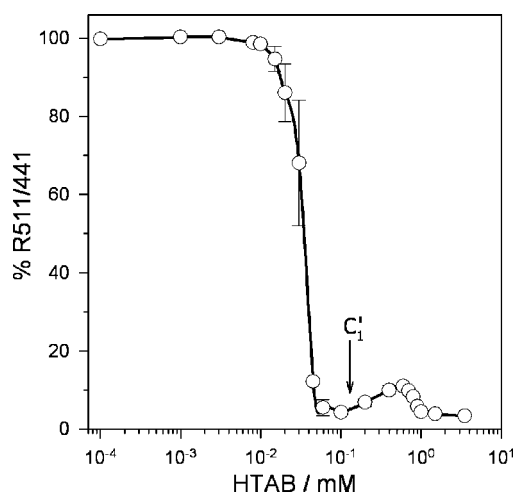


**Figure 8.** Percentage ratio of the fluorescence emission of HPTS at 511 and 441 nm as function of HTAB concentration. After the main decrement of the ratio, a local maximum is observed. (Results: mean  $\pm$  std;  $n \geq 3$ ).

**Effect of the n-Alquiltrimethylammonium Bromide Series on the Steady-state Fluorescence of HPTS.** For the case of TTAB and HTAB in pure water at pH 3.5, the ratio of fluorescence intensities showed similar behavior to DTAB. From the curves, the values of  $C_1$ ,  $C_2$ , and  $C_3$  were determined using the same procedure as that described previously. Experiments with HTAB were also performed at 0.6 and 12  $\mu\text{M}$  of HPTS, leading to values of  $C_1$ ,  $C_2$ , and  $C_3$  that were equivalent to that obtained with 6  $\mu\text{M}$  of dye (see Figure SI.4 in the Supporting Information). Although the main changes in fluorescence spectra caused by both surfactants were similar to those observed with DTAB, two differences were found. First, after the decrease in the  $\% \text{R511/441}$  value to a minimum value due to surfactant concentration, a local increase and a further diminution was observed at higher surfactant concentrations. These increases appeared at a concentration ( $C'_1$ ) of  $0.15 \pm 0.05$  mM for HTAB (Figure 8) and of  $1.28 \pm 0.30$  mM for TTAB (see Figure SI.5 in the Supporting Information). The extent of this local increase rose with the chain length of the surfactant, and the reversal of the phenomenon took place at a surfactant concentration equal to the value of  $C_2$  obtained from the  $\% \text{R511/528}$ . Second, in the case of HTAB, in the concentration range from 0.1 to 1 mM, the changes in fluorescence intensity showed a kinetic

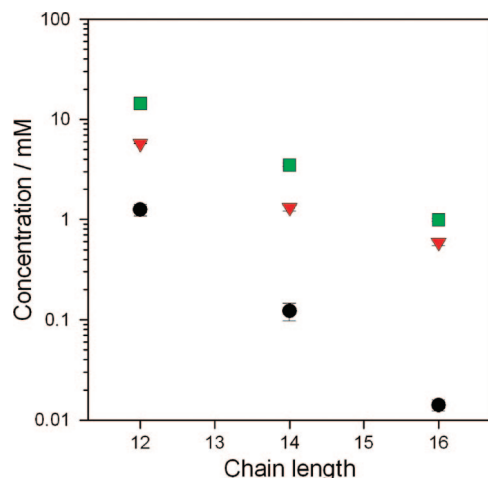


**Figure 9.** Values of  $C_1$  (circle),  $C_2$  (triangle) and  $C_3$  (square) as a function of the chain length of *n*-alkyltrimethylammonium surfactants in water at pH 3.5. (Results: mean  $\pm$  std;  $n \geq 3$ ).

effect. An equilibration time of 5 min was needed to obtain a constant value of fluorescence ratios. Figure 9 shows the concentrations ( $C_1$ ,  $C_2$ , and  $C_3$ ) as a function of the chain length of the surfactants. The corresponding values were  $1.26 \pm 0.17$ ,  $5.74 \pm 0.05$ , and  $14.50 \pm 0.25$  mM for DTAB;  $0.122 \pm 0.024$ ,  $1.32 \pm 0.11$ , and  $3.51 \pm 0.14$  mM for TTAB; and  $0.014 \pm 0.002$ ,  $0.593 \pm 0.042$ , and  $0.995 \pm 0.030$  mM for HTAB. As can be observed, all concentration values diminished with increasing chain length.

#### Effect of SDS and SDoS on spectral properties of HPTS.

The presence of the negative surfactants SDS or SDoS in HPTS solutions at pH 3.5 did not modify the % 511/441 ratio of the samples up to a concentration of approximately 5 mM (see Figure SI.5 in the Supporting Information). This effect was the opposite of that caused by TX100, as, in this case, the higher the surfactant concentration the higher the % 511/441 ratio. This effect diminished with NaCl concentration, and at 300 mM no significant modification in the % ratio was observed. The surfactant concentration did not lead to changes in the R511/528 ratio. The absorption spectra of HPTS did not change as a result of the presence of SDS or SDoS in the aqueous medium.

## 4. Discussion

#### Effect of Triton X-100 on Spectral Properties of HPTS.

As no quenching of HPTS occurs in the presence of TX100, the observed changes in the emission spectra provide evidence that the equilibrium between protonated and deprotonated excited species is modified as a function of the aggregation state of TX100. These changes can be observed by the ratio of  $RO^-*$  and  $ROH^*$  fluorescence emission.

Critical micellar concentration (CMC) is usually calculated from the definition proposed by Phillips:<sup>34</sup> the total concentration of surfactant,  $C$ , corresponding to the maximum change in the gradient of the physical property,  $\psi$ , versus the  $C$  function given in eq 4:

$$\left( \frac{d^3\psi}{dC^3} \right)_{C=cmc} = 0 \quad (4)$$

According to this definition, CMC is commonly determined from the intercept of two straight lines fitting  $\psi$  versus the  $C$  function in the concentration ranges below and above the CMC.

In Figure 1, the maximal change in the physical property occurs at  $C = 0.227 \pm 0.040$  mM, which is equivalent to the values of CMC described in the literature.<sup>35,36</sup> Thus, % R511/441 allows the calculation of the CMC of TX100. The CMC values obtained by this method are independent of NaCl concentration, as expected in the case of nonionic surfactants. TX100 micelles capture water from the surrounding medium by hydrogen bonding with their ether groups—which is considered proper hydration—as well as by osmotic flux and mechanical entrapment caused by the polyoxyethylene chains.<sup>37</sup> Consequently, the hydrogen bonding network of water changes when it becomes associated with micelles. This could explain the variation in the fluorescent spectrum of HPTS when macroaggregates of TX100 are formed. In these conditions, the characteristics of the interaction between the dye and water differ from that in the bulk medium and, in this new microenvironment, the equilibrium among the excited species is modified. The new hydrogen bonds formed between the surfactant and water result in a water restriction to the dye, hence the protonated specie is favored. This behavior has been observed in HPTS solutions containing salts in the molar concentration range.<sup>38</sup> In these cases, the reduction in the effective water concentration also promotes the  $ROH^*$  form. As mentioned by Agmon,<sup>39</sup> HPTS is a weak photoacid that requires additional water molecules in the solvation shell of the  $RO^-*$  species to assist the dissociation process. Then, any diminution of this shell may displace the equilibrium to its  $ROH^*$  form. We hypothesize that there are no strong interactions between the dye and the surfactant and that only the alteration of the aqueous shell of HPTS causes the displacement of the equilibrium. This hypothesis is supported by two complementary facts. First, the absence of fluorescence and absorbance shifts in the corresponding spectra of HPTS and, second, the range of TX100 concentration affecting the fluorescence ratio. Once the TX100 micelles begin to form, the fluorescence properties of the dye change, and this phenomenon occurs progressively for more than 2 orders of magnitude of TX100 concentration. Then, although the dye is in the micromolar range, there is no rapid displacement of the equilibrium of HPTS in bulk to HPTS associated with micelles. In contrast, the ratio of fluorescence diminishes progressively, indicating that the amount of HPTS in the microenvironment caused by the micelles increases gradually as they are formed.

However, in the studied range of NaCl concentrations, the presence of TX100 micelles causes fluorescent ratio curves with an equal slope (Figure 1). This indicates that, from 0 to 300 mM of NaCl, the surfactant has the same effect on the  $ROH^*/RO^-*$  equilibrium. As can be observed for any concentration of NaCl assayed, a given increment of TX100 leads to the same variation of the ratio between the  $ROH^*$  and  $RO^-*$  forms. Molina et al.<sup>37</sup> showed that monovalent cations bind to micelles of TX100 and cause chain dehydration via water–ether bond disruption. Thus, we can conclude that, at the NaCl concentrations tested in our work, there was no alteration in the screening effect of  $Na^+$  on the excited HPTS equilibrium,<sup>40</sup> and, therefore, there was no competition between micelles and HPTS for the cation.

**Effect of Dodecyltrimethylammonium Bromide on the Spectral Properties of HPTS.** Both the absorption and fluorescence spectra of HPTS indicate that DTAB results in major changes in the environment of the dye. Such changes occur in a surfactant concentration range from 0 to 14 mM. From the absorption spectra, it can be stated that, in the ground state, protonated and deprotonated forms of HPTS undergo different type of interactions with DTAB. For example, with



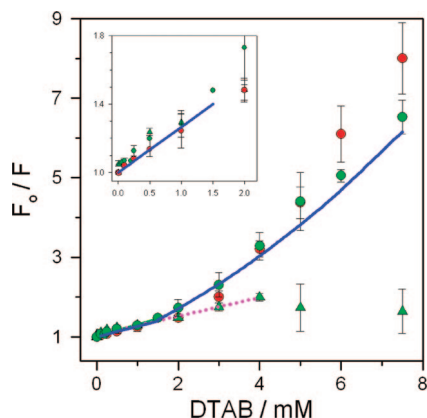


**Figure 10.** Stern–Volmer plot of HPTS fluorescence as a function of DTAB concentration at pH 3.5 (green) and pH 9.4 (red). Circles:  $\text{RO}^{-*}$  form; triangles: ROH form; blue line: adjusted curve calculated taking into account the existence of static quenching between 0 and 1.5 mM and combined quenching between 1.5 and 7.5 mM of DTAB. Inset: detail in the DTAB concentration range from 0 to 2 mM of DTAB.

increasing DTAB concentrations, the ROH absorption spectrum evidences a 2 nm bathochromic shift in the major band located in water at 403 nm (Figure 2a). Simultaneously, there are variations in the absorbance of this peak. However, in the same conditions, the  $\text{RO}^{-}$  spectrum shows, first, a 6 nm bathochromic shift of the 454 nm band and, second, at DTAB concentrations higher than 7 mM, a hypsochromic shift that returns the peak to its initial wavelength (Figure 2b). As for ROH,  $\text{RO}^{-}$  absorption spectrum also exhibits changes in its main absorbance band, which is located at 454 nm in water. These spectral changes can be explained by the formation of a ground-state complex between the dye and the surfactant formed by electrostatic interaction. This complex will be the cause of the static quenching of fluorescent species at either pH 3.5 or 9.4. In this way, the changes in the intensity of the peaks (Figure 3) and of the area of the component bands observed by steady-state fluorescence at pH 3.5 (Table 1 and Figure 4) reveal that, when DTAB concentration is increased from 0 to approximately 1 mM,  $\text{RO}^{-*}$  and  $\text{ROH}^*$  are quenched by the surfactant. This effect takes place in the same way for both species, as there were no significantly different slopes in the Stern–Volmer equation and there was no variation in the % R511/441 (Figure 6). Thus, the presence of the surfactant clearly quenches the same proportion of both species, and, consequently, does not alter the equilibrium between them. As an equivalent variation of the area and intensity of the main peak are obtained in the 0–2 mM range of DTAB when the bulk pH is 9.4, it can be stated that  $\text{RO}^{-*}$  species undergo the same quenching effect as that observed at pH 3.5. Consequently, an average value of the slope is obtained (Figure 10, inset), that is, the static constant  $K_{\text{S}(\text{RO}^{-*})} = 0.266 \pm 0.005 \text{ mM}^{-1}$  (mean  $\pm$  sem). These results are in accordance with the literature, which describes the interaction of HPTS with amino groups<sup>41</sup> of different molecules. Time-resolved data indicate that, for any DTAB concentration below 1–2 mM at pH 3.5 and 9.4, there is no change in the lifetime of  $\text{RO}^{-*}$ . This fact reinforces the assumption that the quenching mechanism of the described process must be static. Consequently, the slopes of the curves correspond to the static association constants,  $K_{\text{S}}$ , between each species and the surfactant. From these results we can infer that, in spite of the different charge of  $\text{RO}^{-}$  and ROH (4 and 3 negative charges, respectively), the quenching of both species between 0 and 1–2 mM of DTAB is equal, that is, it is not a charge-dependent phenomenon. Rosenbluth et al. found similar results when

studying the interaction between alkylpyridinium ions and pyrene derivatives (including HPTS) in aqueous solution.<sup>42</sup> In these cases, quenching of the fluorescent pyrene derivatives was not only independent of the charge of the dye but also of the size of the alkyl chain of the alkylpyridinium cation. In the case of 12 carbon chain length, the above authors reported that pyranine quenching was static, with a constant value of  $5.68 \pm 0.29 \text{ mM}^{-1}$ . They did not find any differences between the premicellar and micellar states of the surfactant. In the present work, the association constants of  $\text{RO}^{-}$  and ROH with DTAB (from 0 to 1–2 mM) are about 20 times smaller, indicating a weaker interaction between HPTS and the surfactant than that found in the case of dodecylpyridinium. For ROH, at pH 3.5 this quenching mechanism takes place up to a maximum DTAB concentration of 4 mM. In contrast, Stern–Volmer plot of the  $\text{RO}^{-*}$  form shows a positive deviation with surfactant concentrations of between 1–2 mM and 7.5 mM (Figures 3 and 10). This decrease in  $\text{RO}^{-*}$  fluorescence causes at pH 3.5 a sharp drop in the % R511/441 plot (Figure 6).

Diverse critical concentrations are commonly determined by using the break or inflection points in a specific physical property of a surfactant, as a function of surfactant concentration.<sup>12,34</sup> In our case, at pH 3.5 the observed break point enabled us to obtain the intersection between the initial value of the ratio (100%) and the tangent to the slope of the curve, that is,  $C_1 = 1.26 \pm 0.17 \text{ mM}$ . This value, which is 1 order of magnitude smaller than the CMC of DTAB, may indicate the formation of premicellar aggregates of DTAB. The existence of similar premicellar aggregates have been reported for dodecyltrimethylammonium cations in the presence of several counterions,<sup>43</sup> and a value of 1.3 mM has been found for dodecyltrimethylammonium hydroxide.<sup>44</sup> Thus, the observed static quenching should be a consequence of the interaction of the dye with monomers of surfactant.

At pH 3.5, from 1 to 7.5 mM of DTAB, the change in % R511/441 does not imply a displacement of the  $\text{ROH}^*/\text{RO}^{-*}$  equilibrium, as was observed in the case of TX100. Here, the reduction in the  $\text{RO}^{-*}$  quantum yield does not lead to an equivalent rise in the corresponding value of  $\text{ROH}^*$  (Figure 4c and Table 1). Consequently, this fact has to be explained by the existence of quenching different to that observed at DTAB concentrations below 1 mM. This quenching is specific to the four negatively charged  $\text{RO}^{-*}$  forms and is caused by nonmicellar aggregated species of DTAB. Although % R511/441 can not be obtained at pH 9.4 at a DTAB concentration lower than 14 mM, the same conclusion is obtained at this basic pH, as no increment of  $\text{ROH}^*$  form is detected during the decrease of the  $\text{RO}^{-*}$  quantum yield.

To establish the type of quenching on  $\text{RO}^{-*}$ , fluorescence lifetimes were determined in the presence ( $\tau$ ) and absence ( $\tau_0$ ) of DTAB. Dynamic quenching has an important characteristic: fluorescence lifetimes are dependent on the quencher concentration ( $\tau_0 \neq \tau$ ). This is not the case in static quenching.<sup>45</sup> Fluorescence lifetime measurements have clearly shown that the quenching caused by DTAB at concentrations ranging from 1–2 mM to 7.5 mM at pH 3.5 and 9.4 has a dynamic nature. From the slope of the  $\tau_0/\tau$  ratio in the aforementioned interval at both pH values, the average constant of dynamic quenching of  $\text{RO}^{-*}$  was obtained,  $K_{\text{D}(\text{RO}^{-*})} = 0.110 \pm 0.010 \text{ mM}^{-1}$ .

The constant of dynamic quenching,  $K_{\text{D}}$ , equals the product of the bimolecular quenching constant,  $k_{\text{q}}$ , and the unquenched lifetime,  $\tau_0$ . Thus, from the above value of  $K_{\text{D}}$  and a mean value of  $5.40 \pm 0.03 \text{ ns}$  for  $\tau_0$ , a bimolecular quenching constant of  $2.04 \times 10^{10} \text{ M}^{-1} \cdot \text{s}^{-1}$  is obtained.



Another characteristic of dynamic quenching is the equivalent decrease in fluorescent intensity and lifetimes ratios, that is:

$$F_0/F = \tau_0/\tau \quad (5)$$

To compare both ratios, a modification of the fluorescent ratio used in the Stern–Volmer equation is required. Thus, the fluorescence,  $F_0$ , corresponding to a DTAB concentration of 1.5 mM was taken as the initial value since this is the center of the experimental concentration range (1–2 mM) at which dynamic quenching caused by DTAB was observed at pH 3.5 and 9.4. However, after this modification, eq 5 could not be accomplished as, for any DTAB concentration higher than 1.5 mM,  $F_0/F > \tau_0/\tau$ . This fact, and the observed upward-curving, suggests that a combined type of quenching is present in the 1.5–7.5 mM interval. In other words, the fluorophore can be quenched both by collisions and by complex formation with the quencher. This behavior has been observed in pyranine/methyl viologen complexes<sup>45</sup> and can be analyzed by means of the following equation:<sup>46</sup>

$$\frac{F_0}{F} = (1 + K_D Q)(1 + K_S Q) \quad (6)$$

where  $K_D$  and  $K_S$  are the dynamic and static quenching constants, respectively, for a given fluorophore. This modified form of the Stern–Volmer equation is second-order in  $[Q]$ , which accounts for the upward curvature observed when both static and dynamic quenching occur in the fluorophore. The previous equation had to be adapted to the previously indicated reference values of fluorescence,  $F_0$ , and concentration, 1.5 mM, and the following equation for the  $RO^{-*}$  form is obtained:

$$\frac{F'_0}{F} = (1 + K_{D(RO^{-*})}([DTAB] - 1.5))(1 + K_{S(RO^{-*})}([DTAB] - 1.5)) \quad (7)$$

where  $K_{S(RO^{-*})} = 0.266 \pm 0.005 \text{ mM}^{-1}$ , and  $K_{D(RO^{-*})} = 0.110 \pm 0.010 \text{ mM}^{-1}$ .

This expression shows a good fit with the experimental values and can be expressed as a function of the initial  $F_0/F$  ratio. Taking into account that at 1.5 mM of DTAB  $F_0/F'_0 = 1.43 \pm 0.17$  (Figure 3), then:

$$\frac{F'_0}{F} = \frac{F_0 F'_0}{F F_0} = \frac{F_0}{F} \frac{1}{1.43} \quad (8)$$

and consequently:

$$\frac{F_0}{F} = 1.43(1 + K_{D(RO^{-*})}([DTAB] - 1.5))(1 + K_{S(RO^{-*})}([DTAB] - 1.5)) \quad (9)$$

This expression is valid for a DTAB concentration between 1.5 and 7.5 mM. As it has been described before, below 1.5 mM of DTAB only static quenching is produced, and a straight line describes the phenomenon. Both approximations are shown in Figure 10, which shows a good fit of the models to the experimental points especially for DTAB concentrations lower

than 6 mM. This fact can be explained by the observed small fluorescence shift of the  $RO^{-*}$  species at DTAB concentrations ranging from 2 to 7.5 mM. This shift, for example, causes the slow decrement of the % R511/528 ratio at DTAB concentrations higher than 3 mM (Figure 7) and is an additional contribution to the diminution of the fluorescence at 511 nm. This fact, obviously, is not considered by the equation of the combined quenching and explains the observed lack of fit.

The effect of DTAB on HPTS can be included in the general interaction shown by the amine group containing dye molecules. Octadecylamine Langmuir–Blodgett films anchor pyranine by its sulfonate groups and modify the equilibrium between the excited species.<sup>3</sup> However, other amino group containing molecules exhibit a quenching effect on HPTS. This is the case of 2,2'-azo-bis(2-aminopropane),<sup>47</sup> DPX (p-xylene-bis-pyridinium bromide)—a symmetrical molecule that contains two amino groups and that is usually employed in analytical fluorescent assays<sup>48</sup>—and the aforementioned alkylpyridinium cations.<sup>42</sup>

At DTAB concentrations above 7.5 mM, the effect of DTAB quenching on the Stern–Volmer plot is hindered by the important shift in the fluorescent bands of HPTS. Consequently, this phenomenon has to be analyzed from the data provided by the area of steady-state spectra. In this concentration range, the relative fluorescent yield (Figure 4) at pH 3.5 and 9.4 shows that the higher the concentration of DTAB, the smaller the quenching effect on HPTS. Quenching is totally eliminated at a surfactant concentration equal to or above 14.5 mM, that is, the CMC of DTAB.<sup>26</sup> Consequently, steady-state fluorescence detects a gradual evolution from the premicellar aggregates of the surfactant to micelles, which do not cause any quenching of the dye. The formation of micelles can be accurately determined using the data in Figure 7, where the tangent of the curve obtained in pure water intersects the minimum ratio of fluorescence (% R511/528) at 14.5 mM. Changes in the fluorescent yield are parallel to that of the  $RO^{-*}$  lifetime and its final value ( $8.79 \pm 0.78 \text{ ns}$  at pH 3.5 and  $6.87 \pm 0.30 \text{ ns}$  at pH 9.4) indicates that in the presence of micelles the dye is in a medium that is less polar than bulk solution.<sup>21</sup> The enhancement of the fluorescence lifetime of pyranine in the presence of HTAB micelles has been described elsewhere.<sup>8</sup>

Moreover, the area of the  $RO^{-*}$  and  $ROH^*$  species show that, when DTAB micelles are formed, there is a rise in concentration of the protonated form in comparison with that observed in pure water (Table 1 and Figure 4, panels c and d). This fact is especially remarkable at pH 9.4, as the  $ROH^*$  species are generated by micelles even though the  $pK^*$  is 1.4.<sup>40</sup> As indicated previously, this effect has also been observed in TX-100 micelles and is a consequence of the decrease in the effective water concentration around the micelles.

Concerning the changes observed in the component bands of the experimental spectra, they can be explained by the creation of a strong electrostatic  $\pi$ -cation interaction between the aromatic rings of HPTS and the headgroups of the surfactant. This kind of interaction has been observed in other dye–surfactant systems,<sup>29,30</sup> showing that it causes the location of a fraction of the fluorophore in a more nonpolar region than the micellar surface of cationic micelles. However, this region is not as hydrophobic as the micellar core. Some dyes, such as Prodan, can, moreover, locate in the micellar core.<sup>30</sup> In our case, the high negative charge of HPTS prevents the movement of the dye through the nonpolar regions composed of the hydrocarbonated chains found in the micellar core or bilayers.<sup>48</sup> Consequently, the observed shifts in the experimental curves,

caused by the new component bands located at about 420 and 550 nm, are consistent with the location of the dye in an environment other than the hydration sphere of the micelle, due to  $\pi$ -cation interaction. The observed shifts can be explained by taking into account the modification of the hydrogen bonds established, in the absence of micelles, between the dye and the water. The main hydrogen bond formed by protonated photoacids is created with a solvent molecule.<sup>39</sup> This bond stabilizes the excited-state more than the ground state. The emission spectrum shows a red shift that becomes larger as the hydrogen bond strength increases. Thus, the location of HPTS in a medium that is less polar than water, driven by the  $\pi$ -cation interaction, leads to a reduction in the number of hydrogen bonds formed previously between water and ROH\*. This leads to an increment in the energetic difference between the excited and ground states of the molecule, that is, a reversal of the red shift. This is confirmed by the blue shift observed in the ROH\* band that, in turn, is a result of the new component band of the spectrum centered at 422 nm. Concerning the solvatochromism of deprotonated photoacids, Agmon indicates that, unlike the acid form, the anion interacts with the hydrogen bond with donating solvents. In this case, stabilization is greater in the ground-state than in the excited state, leading to a blue shift.<sup>39</sup> The observed effect of deprotonated HPTS is, again, a result of the location of the dye in micelles as a consequence of  $\pi$ -cation interaction. This prevents the formation of hydrogen bonds between RO<sup>-</sup>\* and the donating solvent (water) and, therefore, results in a reduction in the energy between the excited and ground state, that is, a red shift of the RO<sup>-</sup>\* band caused by the component band located at approximately 550 nm. It is clear that, at any of the assayed pH, the location of the deprotonated dye in the less polar medium such as micelles favors its reprotonation (no protonated HPTS in the ground-state is detected by absorbance). This fact allows the existence of the protonated excited state, at least, from 2 to 8 pH units above its  $pK^*$  in water.

**Effect of n-Alquiltrimethylammonium Bromide Series on Steady-state Fluorescence of HPTS.** The values of CMC (or  $C_3$ ) obtained for the dodecyl-, tetradecyl-, and hexadecyl-alquiltrimethylammonium bromides,  $14.50 \pm 0.25$ ,  $3.51 \pm 0.14$ , and  $0.995 \pm 0.030$  mM, respectively, are in agreement with the literature.<sup>21,28,49</sup> The observed variation of CMC with chain length is a well-known phenomenon<sup>12</sup> and confirms that HPTS is a suitable dye for determining this characteristic parameter for this type of surfactants. In relation to the influence of salts on the CMC of DTAB, values of  $C_3$  are also in an acceptable agreement with the literature. For instance, in the presence of 13 mM of NaCl a CMC of 10.7 mM is found,<sup>50</sup> and after applying eq 3, a value of 11.9 was obtained. The  $C_2$  and  $C_3$  values also show the same type of variation with chain length and allow the evolution of the systems from monomers to micelles to be characterized. Regarding HTAB, the calculated  $C_2$  ( $0.593 \pm 0.042$  mM) is similar to reported data.<sup>21,51,52</sup> However, the first critical concentration,  $C_1$  ( $0.014 \pm 0.002$  mM), does not match the literature as it is about 1 order of magnitude lower. The values described in the literature were obtained by fluorimetric methods and are the same as those obtained in Figure 8, if a local maximum of % R511/441 is considered. Here the second change of the ratio value was initiated between 0.1 and 0.2 mM of HTAB ( $C'_1$ ), that is, the same interval as that found by other authors for  $C_1$ . Consequently, our results suggest that for TTAB and HTAB four critical concentrations can be calculated with high precision using HPTS. In our work, special attention has been focused

on a wide interval of surfactant concentrations, allowing detailed representations of the fluorescent changes with semilogarithmic plots to be obtained. Our results are a consequence of variation in fluorescent ratios. We did not assess absolute fluorescence changes. This could explain the differences found with the previous works, in which  $C_1$  may not have been detected because small changes of the probe fluorescent intensity were not assessed. As far as can be observed from the published graphics, few experimental points were found in the lower concentration range of the surfactant.

#### Effect of SDS and SDoS on Spectral Properties of HPTS.

A minor increment in the fluorescence intensity ratio (R511/441) of HPTS in water in the presence of negative surfactants is in contrast to that observed with cationic and nonionic surfactants, in which a decrease was observed. The presence of atomic cations modifies the equilibrium between excited species of HPTS.<sup>40</sup> If it is taken into account that negative surfactants are sodium salts, the increment of the ratio at high surfactant concentrations can be explained by the effect of the counterion. This also explains the fact that the changes in the intensity ratio observed in pure water are progressively eliminated when NaCl concentration increases: in these cases, the sodium cation present in the aliquot of the stock solution of surfactant added to the sample is a small part of the total. These results suggest that HPTS does not interact with anionic surfactants; probably due to high electrostatic repulsion. This repulsion is not eliminated until a NaCl concentration of at least 300 mM is reached.

## 5. Conclusions

The present study reports the extent of the photophysical changes undergone by HPTS when it interacts with differently charged surfactants. In the presence of anionic SDS and SDoS, electrostatic repulsion prevents any kind of interaction. Micelles of the nonionic TX-100 produce spectral changes as a consequence of the shift in the equilibrium of its excited species. However, in the presence of cationic n-alquiltrimethylammonium bromides, the behavior of the dye, in relation to that observed in the bulk aqueous phase, is dramatically modified. The sensitivity of HPTS to the polarity of its microenvironment enables a rich complexity of surfactant aggregates to be detected. In this way, it is possible to use fluorescence changes to follow the formation of premicellar aggregates of the three cationic surfactants assayed and their subsequent evolution to micelles. Such an evolution has been characterized by three critical concentrations that show their dependence on the chain length of the surfactant. In the case of DTAB, the interaction of HPTS evidence a quenching effect that displays a different nature (static or combined), depending on the surfactant concentration. Spectral results have produced compelling evidence that, in the presence of micelles, HPTS is located in its aqueous hydration layer and also in a more nonpolar region. This location could be due to a  $\pi$ -cation interaction. Such interactions cause a shift in the emission band of both protonated and deprotonated excited HPTS, as a result of the modification of the hydrogen bonds previously formed with water molecules.

**Acknowledgment.** The authors thank the Ministerio de Educación y Ciencia, Plan Nacional de Investigación, Desarrollo e Innovación Tecnológica (I+D+i) for financial support in project MAT2006-12918-C05-05.

**Supporting Information Available:** Relative intensity absorbance peaks of HPTS, fluorescence lifetimes decays of deprotonated HPTS, effect of HPTS concentration on fluorescent

ratios, % R511/528 of HPTS in presence of DTAB or TTAB at different concentration at different pH, and the % R511/441 fluorescence ratio of HPTS as a function of SDS concentration at different NaCl concentrations. This information is available free of charge via the Internet at <http://pubs.acs.org>.

## References and Notes

- (1) Pines, E.; Huppert, D.; Agmon, N. *J. Chem. Phys.* **1988**, *88*, 5620.
- (2) Ghosh, S.; Dey, S.; Mandal, U.; Adhikari, A.; Mondal, S. K.; Bhattacharyya, K. *J. Phys. Chem. B* **2007**, *111*, 7085.
- (3) Ray, K.; Nahakara, H. *J. Photochem. Photobiol. A: Chem.* **2005**, *173*, 75.
- (4) Barrash-Shiftan, N.; Brauer, B.; Pines, E. *J. Phys. Org. Chem.* **1998**, *11*, 743.
- (5) Politi, M. J.; Fendler, J. H. *J. Am. Chem. Soc.* **1984**, *106*, 265.
- (6) Scherrer, P.; Alexeiev, U.; Marti, T.; Khorana, H. G.; Heyn, M. P. *Biochemistry* **1994**, *33*, 13684.
- (7) Alexeiev, U.; Marti, T.; Heyn, M. P.; Khorana, H. G.; Scherrer, P. *Biochemistry* **1994**, *33*, 13693.
- (8) Roy, D.; Karmakar, R.; Mondal, S. K.; Sahu, K.; Bhattacharyya, K. *Chem. Phys. Lett.* **2004**, *399*, 147.
- (9) Sahu, K.; Roy, D.; Mondal, S. K.; Karmakar, R.; Bhattacharyya, K. *Chem. Phys. Lett.* **2005**, *404*, 341.
- (10) Pramanik, S.; Banerjee, P.; Bhattacharyya, S. C. *J. Photochem. Photobiol. A: Chem.* **2007**, *187*, 384.
- (11) Lawrence, M. J. *Chem. Soc. Rev.* **1994**, *23*, 417.
- (12) Evans, D. F.; Wenneström, H. *The Colloidal Domain Where Physics, Chemistry, Biology, and Technology Meets*; VCH Publishers: New York, 1994.
- (13) Zettl, H.; Portnoy, Y.; Gottlieb, M.; Krausch, G. *J. Phys. Chem. B* **2005**, *109*, 13397.
- (14) Niu, S.; Gopidas, K. R.; Turro, N. J.; Gabor, G. *Langmuir* **1992**, *8*, 1271.
- (15) Karukstis, K. K.; Savin, D. A.; Loftus, C. T.; D'Angelo, N. D. *J. Colloid Interface Sci.* **1998**, *203*, 157.
- (16) Sabaté, R.; Gallardo, M.; Estelrich, J. *Electrophoresis* **2000**, *21*, 481.
- (17) Junquera, E.; Arranz, R.; Aicart, E. *Langmuir* **2004**, *20*, 6619.
- (18) del Burgo, P.; Aicart, E.; Junquera, E. *Colloids Surf. A* **2007**, *292*, 165.
- (19) Aicart, E.; del Burgo, P.; Llorca, O.; Junquera, E. *Langmuir* **2006**, *22*, 4027.
- (20) del Burgo, P.; Aicart, E.; Llorca, O.; Junquera, E. *J. Phys. Chem. B* **2006**, *110*, 23524.
- (21) Jaffer, S. S.; Sowmiya, M.; Saha, S. K.; Purkayastha, P. *J. Colloid Interface Sci.* **2008**, *325*, 236–242.
- (22) Hadgiiivanova, R.; Diamant, H. *J. Phys. Chem. B* **2007**, *111*, 8854.
- (23) Buwalda, R. T.; Jonker, J. M.; Engberts, J. B. F. N. *Langmuir* **1999**, *15*, 1083.
- (24) Wong, J. E.; Duchsherer, T. M.; Pietraru, G.; Cramb, D. T. *Langmuir* **1999**, *15*, 6181–6186.
- (25) Sabaté, R.; Gallardo, M.; de la Maza, A.; Estelrich, J. *Langmuir* **2001**, *17*, 6433.
- (26) Sabaté, R.; Estelrich, J. *J. Phys. Chem. B* **2003**, *107*, 4137.
- (27) Karukstis, K. K.; Zieleniuk, C. A.; Fox, M. J. *Langmuir* **2003**, *19*, 10054.
- (28) Matzinger, S.; Hussey, D. M.; Fayer, M. D. *J. Phys. Chem. B* **1998**, *102*, 7216.
- (29) Sabaté, R.; Gallardo, M.; Estelrich, J. *J. Colloid Interface Sci.* **2001**, *233*, 205.
- (30) Karukstis, K. K.; McDonough, J. R. *Langmuir* **2005**, *21*, 5716–5721.
- (31) Junquera, E.; del Burgo, P.; Boskovic, J.; Aicart, E. *Langmuir* **2005**, *21*, 7143.
- (32) Huppert, D.; Kolodney, E.; Gutman, M.; Nachliel, E. *J. Am. Chem. Soc.* **1982**, *104*, 6949.
- (33) Wolfbeis, O. S.; Furlingerr, E.; Kroneis, H.; Marsoner, H. *Fresen. J. Anal. Chem.* **1983**, *314*, 119.
- (34) Phillips, J. N. *Trans. Faraday Soc.* **1955**, *51*, 561.
- (35) Tadros, Th. F. *Applied Surfactants. Principles and Applications*; Wiley-VCH: Weinheim, 2006.
- (36) Hinze, W. L. *Ann. Chim.* **1987**, *77*, 167.
- (37) Molina-Bolívar, J. A.; Aguiar, J.; Carnero Ruiz, C. J. *Phys. Chem. B* **2002**, *106*, 106.
- (38) Leiderman, P.; Gepshtein, A.; Uritski, A.; Genosar, L.; Huppert, D. *J. Phys. Chem. A* **2006**, *110*, 5573.
- (39) Agmon, N. *J. Phys. Chem. A* **2005**, *109*, 13.
- (40) Barnadas-Rodríguez, R.; Estelrich, J. *J. Photochem. Photobiol. A: Chem.* **2008**, *198*, 262.
- (41) Sharma, J.; Tlegabulova, D.; Czardybon, W.; Brennan, J. D. *J. Am. Chem. Soc.* **2006**, *128*, 5496.
- (42) Rosenbluth, H.; Weiss-López, B.; Olea, A. F. *Photochem. Photobiol.* **1997**, *66*, 802.
- (43) Kale, K. M.; Cussler, E. L.; Evans, D. F. *J. Soln. Chem.* **1982**, *11*, 581.
- (44) Schulz, P. C.; Morini, M. A.; Minardi, R. M.; Puig, J. E. *Colloid Polym. Sci.* **1995**, *273*, 959.
- (45) de Borja, E. B.; Amaral, C. L. C.; Politi, M. J.; Villalobos, R.; Baptista, M. S. *Langmuir* **2000**, *16*, 5900.
- (46) Lakowicz, J. R. *Principles of Fluorescence Spectroscopy*; Kluwer Academic/Plenum: New York, 1999.
- (47) Pino, E.; Campos, A. M.; Lissi, E. *J. Photochem. Photobiol. A: Chem.* **2003**, *155*, 63.
- (48) A Guide to Fluorescent Probes and Labeling Technologies, url: <http://probes.invitrogen.com/handbook/> (accessed 1/2009).
- (49) Ródenas, E.; Dolcet, C.; Valiente, M.; Valerón, E. C. *Langmuir* **1994**, *10*, 2088.
- (50) Hiemenz, P. C.; Rajagopalan, R. *Principles of Colloid and Surface Chemistry* 3rd Ed.; Marcel Dekker: New York, 1997.
- (51) Chaudhury, R.; Guharay, J.; Sengupta, P. K. *J. Photochem. Photobiol. A: Chem.* **1996**, *101*, 241.
- (52) Mallick, A.; Haldar, B.; Maiti, S.; Chattopadhyay, N. *J. Colloid Interface Sci.* **2004**, *278*, 215.

JP806808U